Modeling and Analysis of Variable Frequency One-Cycle Control on High-Power Switched-Capacitor Converters

Bin Wu, *Student Member, IEEE*, Lei Yang, *Student Member, IEEE*, Xiaobin Zhang, Keyue Ma Smedley, *Fellow, IEEE*, and Guann-pyng Li, *Member, IEEE*

***Abstract*—Switched-capacitor (SC) converter is a type of variable structure systems. SC converters are typically equipped with open-loop control or some linear feedback control methods. However, these approaches provide slow dynamic response speed, small operation region, and large voltage ripple. Some new nonlinear control methods have been proposed in the literature to overcome these barriers. However, such control methods are usually proposed for applications involving low-power SC converters due to the limitations of them. This paper presents a nonlinear constant on-time variable frequency one-cycle control (CVFOCC) strategy based on dynamic capacitor ampere-second balance transient calculation (CASBTC) modeling method and one-cycle control (OCC) technique for high-power SC converters. This method successfully addresses the regulation issue of high-power SC converters. A high-power 3X Two-switch Boosting Switched-Capacitor converter (TBSC) is employed as an example topology. Simulation and experimental results both demonstrate that CVFOCC method could significantly improve the dynamic response speed and achieve excellent line and load regulation for the high-power SC converter in wide operation range.**

***Index Terms*—Dynamic capacitor ampere-second balance transient calculation (CASBTC), high power, one-cycle control (OCC), two-switch boosting switched-capacitor (TBSC) converter.**

I. Introduction

DUE to the advantages of light weight, small size, high power density, and absence of inductive elements, switched-capacitor (SC) converters have been widely used in low-power applications [1]–[3]. There are different kinds of control methods for regulation of SC converters investigated under low-power applications from several milliwatts to tens of watts. The most popular methods are pulse width modulation (PWM) [4]–[5], current source [6]–[8] modulation, and frequency modulation (FM) [9]–[11]. As shown in papers [4] and [5], due to the symmetrical structure of power stage of SC converters, the duty-cycle should be limited below 0.5, which is required to prevent the overlap of control signals (e.g., in high-power area) for different switches in SC converters. As shown in [12], for SC converters, the current at charging or discharging phases is decaying exponentially and system conversion ratio is $M(D) = \frac{K(1-e^{\frac{-DT}{RC}})}{(1-e^{\frac{-DT}{RC}})[1-\frac{T}{2}(R+R_L)C]}$. The nonlinear characteristic of SC converters challenges the controller design. In an SC converter, the time constant τ of the charge loop is typically small [13]. To achieve effective regulation, it is necessary for a controller to ensure the turn-on time of a transistor below the time constant τ of charging loop. As a result, the conventional linear control method is forced to work in a narrow operation region [14]. Recently, some nonlinear control methods have been proposed to achieve wider operation range and better dynamic performance. The variable structure control (VSC) (i.e., the sliding control method in [13]) based on energy balance principle was proposed in [12], which established the fact that nonlinear approaches could improve the dynamic and steady-state performance of SC converters. However, with this control method, it is necessary to assure the existence and stability conditions of the sliding mode operation. Another control method that adopted adaptive mixed-on time and variable frequency control to reduce input current spike was provided in [15]. It was used in the interleaving SC cells to achieve seamless charging current from power source.

When it comes to the high-power SC converters, the voltage regulation is more challenging due to the high-peak pulsating current and the stress limitations of semiconductor devices [16]. So far, the major research activities have been mainly focused on the topologies of high-power SC converters [17]–[20]. Unregulated open-loop control method was adopted to achieve high efficiency, convenience, and low cost in [16] and [21]. The output voltage was established by a fixed voltage ratio. In some literature [22]–[23], inductive elements along the charge and discharge loops were introduced to change a SC converter to be a resonant switched-capacitor Converter (RSC) to mitigate current pulsation but still with fixed gain. The inductive element is helpful to suppress the peak charging current and

Manuscript received March 8, 2017; revised June 3, 2017; accepted July 21, 2017. Date of publication August 8, 2017; date of current version February 22, 2018. Recommended for publication by Associate Editor R. C. N. Pilawa-Podgurski. *(Corresponding author: Lei Yang.)*

B. Wu is with the Maxim Integrated, San Jose, CA 95134 USA (e-mail: binw1@uci.edu).

L. Yang is with the School of Automation and information Engineering, Xi'an University of Technology, Xi'an 710048, China (e-mail: yanglei0930@gmail.com).

X. Zhang is with the School of Automation, Northwestern Polytechal University, Xi'an 710072, China (e-mail: dgl907@126.com).

K. M. Smedley and G.-p. Li are withthe Department of Electrical Engineering and Computer Science, University of California, Irvine, Irvine, CA 92617 USA (e-mail: smedley@uci.edu; gpli@uci.edu).

Color versions of one or more of the figures in this paper are available online at http://ieeexplore.ieee.org.

Digital Object Identifier 10.1109/TPEL.2017.2737469

reduce the stress of components. Effort has been made to introduce the close-loop voltage regulation for the high-power SC converter. The high-power two-switch boosting switched-capacitor (TBSC) converter has been proposed in [24]–[26], which demonstrated high efficiency (97.5% peak efficiency) with the soft rising edge input current. Based on the charge-balance transient-calculation (CT) modeling method and current stress estimation, the output voltage regulation for 3X TBSC converter was achieved by using proportional–integral (PI) control method. However, the performance on the response speed, line and load regulation, and operation range of the TBSC converter could be improved by introducing a nonlinear control method. The large-signal nonlinear one-cycle control (OCC) method was proposed in [27]–[31], which is capable of rejecting the external disturbance through one switching cycle and is widely used in the traditional inductor-based converters. The duty ratio d of a switch is controlled such that in each switching cycle the average value of controlled variable in a converter is exactly equal to or proportional to the control reference in the steady-state. This control concept is straightforward with simple implementation circuit featuring in one cycle response speed, robust performance, and automatic switching error correction.

A constant on time ("on time" is smaller than the time constant τ of charging loop) variable frequency nonlinear one-cycle control method (CVFOCC) for the high-power TBSC converter is proposed in this paper. It provides the superior regulation performance in a wide operation range. Moreover, it provides constant and controllable input peak current under variable load conditions.

II. Modeling and Development of CVFOCC Method for TBSC Converter

A. Modeling Methods for SC Converters

There are different modeling methods for SC converters. The state-space averaging model for SC converters was adopted in [32] and [33] to obtain the converter voltage ratio. This modeling method was originally developed for the conventional inductor-based converter. However, the steady-state model of SC converters can be represented by derivation of the "equivalent output equivalent resistance." Average-current-based conduction loss model was shown in [34] and [35], this modeling method takes into account both duty cycle and frequency effects on equivalent output impedance. The slow and fast switching limit model was developed in [36]. Based on energy conservation, the equivalent output impedance of SC converters was calculated in slow frequency or fast frequency end respectively. The work in [34] was the extension of [36]. The modeling result in the area between fast switching and slow switching limits was also explored in [34]. The charge-balance transient calculation modeling method was proposed in [24]. The flying capacitance, loop resistance, duty cycle, and frequency are all addressed in its modeling result. This modeling method provides prediction of circuit behaviors at variable duty cycle and frequency conditions. In [37], the static model of SC converters was expanded by including the dynamic behavior at the input voltage change and reference steps. This modeling method successfully addressed both transient and static conditions. Based on discussions above and different modeling methods, a dynamic CASBTC modeling method is proposed which yields accurate transient prediction of TBSC converter. In combination with CVFOCC method, the TBSC converter can be properly regulated in wide operation range with robust performance.

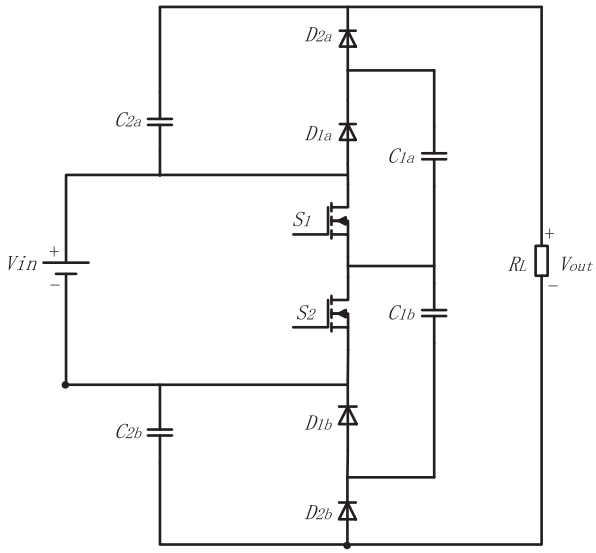

Fig. 1. Topology of 3X TBSC Converter.

B. Modeling of 3X TBSC Converter With CASBTC Method

The 3X TBSC converter is shown in Fig. 1 and its equivalent operation circuits are shown in Fig. 2. With CASBTC modeling method, this 3X TBSC converter has two operation states as shown in Fig. 2 (a) and (b). In State 1, when switch S_1 is ON and switch S_2 is OFF, the flying capacitor C_{1b} is charged by the power source for T_{on} time period. During the same time period, the flying capacitor C_{1a} releases its stored energy to capacitor C_{2a}.The series connected power source, capacitors C_{2a} and C_{2b} sustain the output voltage and power the load resistor. On the other hand, in State 2, when switch S_2 is ON and switch S_1 is OFF, the flying capacitor C_{1a} is charged by the power source for T_{off} time period. During the same time period, the flying capacitor C_{1b} discharges its stored energy to capacitor C_{2b}.The series connected power source, capacitors C_{2a} and C_{2b} again support the output voltage together to power the load resistor.

C_{1b} and C_{2a} are concurrently charged for T_{on} time period during State 1 through switch S_1.On the other hand, C_{1a} and C_{2b} are simultaneously charged for T_{off} time period during State 2 through switch S_2. In one switching cycle, the load resistor is continuously absorbing power through the series connected power source, C_{2a} and C_{2b}. In order to facilitate the modeling construction and analysis, the following assumptions are made:

1) assume switches S_1 and S_2 are identical with the same "on resistance" ($R_{s1} = R_{s2}$);
2) assume flying capacitors C_{1a}, C_{1b}, C_{2a}, and C_{2b} are identical with the same capacitance ($C_{1a} = C_{1b} = C_{2a} = C_{2b} = C$) and same equivalent series resistance ($R_{c1a} = R_{c1b} = R_{c2a} = R_{c2b} = R_c$);

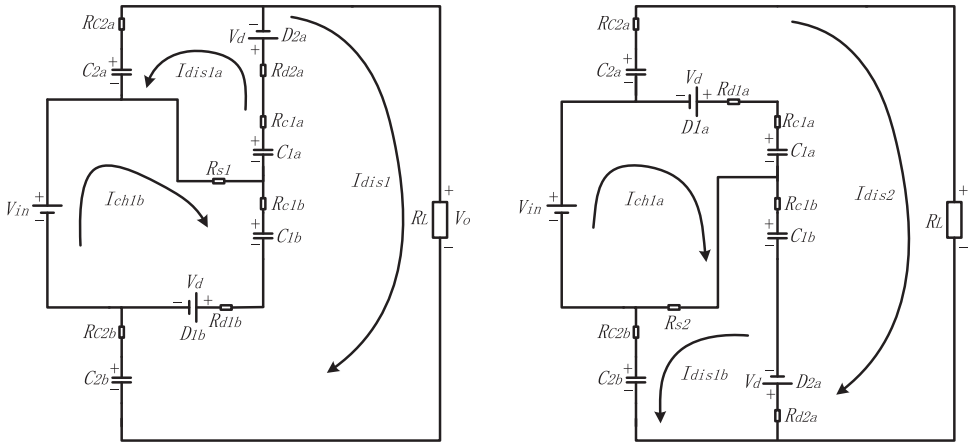

Fig. 2. Equivalent circuits of two operation states for 3X TBSC converter (a) State 1 [0, T_{on}]; (b)State 2 [T_{on}, T_s].

3) assume diodes D_{1a}, D_{1b}, D_{2a}, and D_{2b} are identical with the same "on resistance" ($R_{d1a} = R_{d1b} = R_{d2a} = R_{d2b} = R_d$);
4) the forward voltages of diodes D_{1a}, D_{1b}, D_{2a}, and D_{2b} and internal resistance of power source are neglected;
5) when switch S_1 is ON, switch S_2 must be OFF and vice versa.

During charging period (State 1) of C_{1b}, as shown in Fig. 2(a), C_{1b} is charged by the power source. Based on Kirchhoff's Voltage Law (KVL), the instantaneous charging current of C_{1b} can be estimated as

$$I_{\text{ch1}b}(t) = \frac{V_{\text{in}} - V_{c1b}(t)}{2R_{s1} + R_{d1b} + R_{c1b}} = C\frac{dV_{c1b(t)}}{dt} \tag{1}$$

where V_{in} is input voltage, and $V_{c1b}(t)$ is instantaneous voltage of C_{1b} in State 1.

Considering (1), the charge of C_{1b} during State 1 can be derived as

$$Q_{\text{charge}} = I_{\text{ch1}b}(t)\,T_{\text{on}} = \int_0^{T_{\text{on}}} \frac{V_{\text{in}} - V_{c1b}(t)}{R_{s1} + R_{d1b} + R_{c1b}}dt \tag{2}$$

where T_{on} is the "on time" of switch S_1.

In one switching cycle, based on KVL, the instantaneous load current of 3X TBSC converter can be derived as

$$I_{o(t)} = \frac{V_o(t)}{R_L} = \frac{(V_{\text{in}} + V_{c2a}(t) + V_{c2b}(t)) - V_o(t)}{R_{c2a} + R_{c2b}} \tag{3}$$

where $V_o(t)$ is instantaneous output voltage, $V_{c2a}(t)$ is instantaneous voltage of C_{2a}, and $V_{c2b}(t)$ is instantaneous voltage of C_{2b}.

During the discharging period (State 2) of C_{1b}, as shown in Fig. 2(b), C_{1b} discharges its stored energy to C_{2b}. Since the charge delivered to load will be first stored in intermediate flying capacitor C_{1b} as shown in [24] and [26], the negative discharge of C_{1b} during discharging period can be expressed as

$$-Q_{\text{discharge}} = -I_{\text{dis1}b}(t)\,T_{\text{off}} = I_o(t)\,(T_{\text{on}} + T_{\text{off}}) \tag{4}$$

where $I_{\text{dis1}b}(t)$ is instantaneous discharging current of C_{1b} in State2. T_{off} is the "off time" of switch S_1.

Substitute (3) into (4) and assume the discharging period of C_{1b} is linear, (4) can be rearranged as

$$-Q_{\text{discharge}} = \frac{\left(V_{\text{in}} + V_{c2a}(t) + V_{c2b(t)}\right) - V_o(t)}{R_{c2a} + R_{c2b}}(T_{\text{on}} + T_{\text{off}}). \tag{5}$$

The one switching cycle dynamic capacitor ampere-second balance of C_{1b} can be expressed as

$$Q_{\text{charge}} = I_{\text{ch1}b}(t)\,T_{\text{on}} = -Q_{\text{discharge}} = I_o(t)\,(T_{\text{on}} + T_{\text{off}}). \tag{6}$$

Submitting (2) and (5) into (6), the (6) can be rewritten as

$$\int_0^{T_{\text{on}}} \frac{V_{\text{in}} - V_{c1(b)}}{2R_{s1} + R_{d1b} + R_{c1b}}dt = \frac{(V_{\text{in}} + \overline{V_{c2a}(t)} + \overline{V_{c2b}(t)}) - V_o}{R_{c2a} + R_{c2b}}(T_{\text{on}} + T_{\text{off}}). \tag{7}$$

Replacing $(V_{\text{in}} + \overline{V_{c2a}(t)} + \overline{V_{c2b}(t)})$ by the reference voltage V_{ref} and letting $\partial_1 = \frac{1}{2R_{s1} + R_{d1b} + R_{c1b}}$ and $\partial_2 = \frac{1}{R_{c2a} + R_{c2b}}$, the (7) could be rearranged as

$$\partial_1 \int_0^{T_{\text{on}}} (V_{\text{in}} - V_{c1b}(t))dt = \partial_2\,(V_{\text{ref}} - V_o)\,(T_{\text{on}} + T_{\text{off}}). \tag{8}$$

Using the similar analysis principle for C_{1a} and letting $\beta_1 = \frac{1}{2R_{s2} + R_{d1a} + R_{c1a}}$ and $\beta_2 = \frac{1}{R_{c2a} + R_{c2b}}$, the one switching cycle dynamic capacitor ampere-second balance of C_{1a} can be derived as

$$\beta_1 \int_{T_{\text{on}}}^{T_s} (V_{\text{in}} - V_{c1a}(t))\,dt = \beta_2\,(V_{\text{ref}} - V_o)\,(T_{\text{on}} + T_{\text{off}}). \tag{9}$$

The output voltage conversion ratio based on CASBTC modeling method is derived as (10) shown at the bottom of the next page, where, $R_{\text{ch}} = R_s + R_d + R_c$ and $R_{\text{dis}} = R_s + R_d + 2R_c$.

For the detailed derivation, refer to Appendix.

The 3X TBSC converter can be controlled by the proposed control method with the modeling equations (8) or (9). In this control method, the transistor is adjusted by constant T_{on} and variable T_{off}. It can be observed from the modeling equations (8) and (9), the instantaneous value of input voltage, voltage of the

flying capacitor, output voltage, and one switching cycle time period T_s ($T_s = T_{\text{on}} + T_{\text{off}}$) are all included in the modeling equations. As a result, the external disturbance in the power source and load can be immediately rejected by adjusting the turn off time which effectively changes the switching frequency and duty cycle simultaneously. The "control signals overlap" rejection can be achieved by setting a smaller "on time" T_{on} compared to the time constant τ of the charge loop of C_{1b}. On the other hand, the operation of the current state is independent to the history states by using a resettable integrator which will be presented in the controller circuit.

III. Operation Principle of CVFOCC Method for TBSC Converter

A. CVFOCC Technique

In this paper, the CVFOCC method is constructed in combination with 3X TBSC converter. As C_{1a} and C_{1b} deliver same amount of charge during one cycle, it is only needed to consider the dynamic capacitor ampere-second balance of C_{1b}.The proposed control method maintains constant T_{on} time period of switch S_1 in Fig. 1. The output voltage regulation is achieved by changing T_{off} time period of switch S_1. The frequency of control signals of S_1 (U_{s1}) and S_2 ($U_{s2} = \overline{U_{S_1}}$) are determined by the key control equation (8). The operating waveforms of dynamic capacitor ampere-second balance of C_{1b} are shown in Fig. 3(a).

The operation mechanism of CVFOCC technique for rejecting the external disturbance is shown in Fig. 3(b) and (c). In Fig. 3(b), the input voltage experiences a voltage step-up function, whereas the load current $I_o(t) = \frac{(V_{\text{in}} + V_{c2a(t)} + V_{c2b}(t)) - V_o}{2R_c}$ and reference voltage are kept constant. At the moment of input voltage stepping-up, the charging current $I_{\text{ch}1b}(t) = \frac{V_{\text{in}} - V_{c1b}(t)}{R_{s1} + R_d + R_c}$ will increase immediately. Since T_{on} of switch S_1 is maintained constant, the charge of capacitor C_{1b} will increase correspondingly. Based on dynamic capacitor ampere-second balance principle ($Q_{\text{charge}} = -Q_{\text{discharge}}$), the "turn-off" time will increase, leading to a lower switching frequency compared with previous state. While, if the input voltage experiences a step-down function, T_s. will decrease. The corresponding switching frequency will become higher than previous state.

In Fig. 3(c), a step-up disturbance is introduced at the load current, whereas the input voltage and reference voltage are maintained constant. As a result, the delivered charge Q_{charge} of C_{1b} at charging state is kept constant. Similar to the rejection to the input voltage disturbance, based on the dynamic capacitor ampere-second balance principle ($Q_{\text{charge}} = -Q_{\text{discharge}}$), T_s will be shortened. Therefore, the corresponding switching frequency is increased to maintain the output voltage. Similarly, if the load current steps down, T_s will increase and the related switching frequency will become lower than previous state.

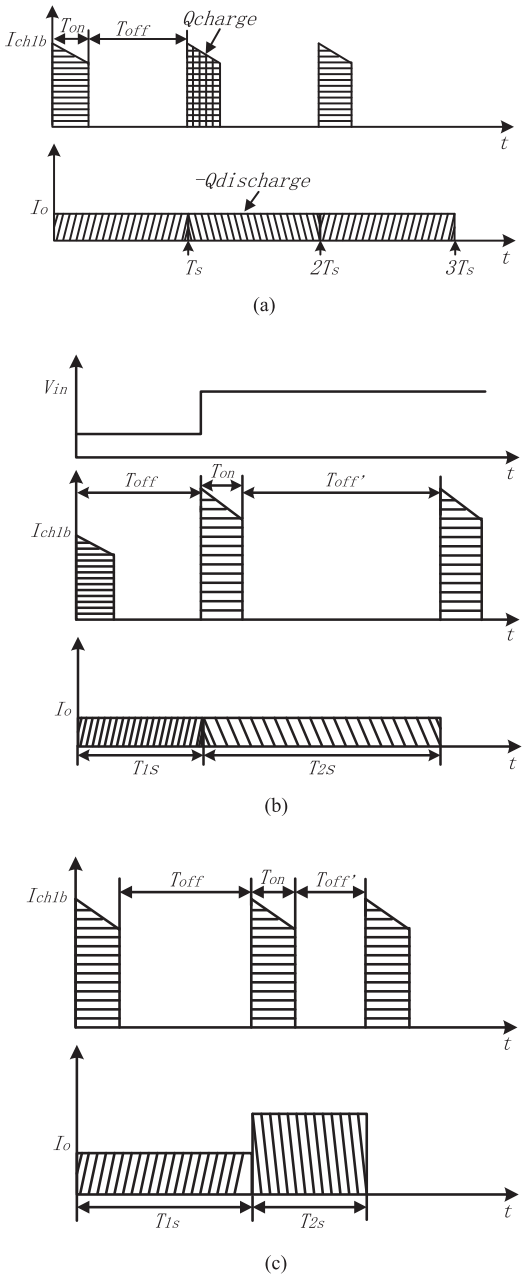

Fig. 3. Operation waveforms of charging currents of C_{1b} and load current of 3X TBSC converter (a) without disturbance. (b) Input voltage (step-up) perturbation rejection with CVFOCC method. (c) Load current (step-up) disturbance rejection with CVFOCC method.

$$\frac{V_o}{V_{\text{in}}} = \frac{6R_L C}{2R_L C + 2(T_{\text{on}} + T_{\text{off}})\left(\frac{1}{\left(1 - e^{\frac{-T_{\text{off}}}{R_{\text{ch}}C}}\right)} + \frac{1}{\left(1 - e^{\frac{-T_{\text{on}}}{R_{\text{ch}}C}}\right)}\right) + 2R_{\text{dis}}C + 2\left[\frac{(2T_{\text{on}} + T_{\text{off}})}{\left(1 - e^{\frac{-2T_{\text{off}}}{R_{\text{dis}}C}}\right)} + \frac{(2T_{\text{off}} + T_{\text{on}})}{\left(1 - e^{\frac{-2T_{\text{on}}}{R_{\text{dis}}C}}\right)}\right] - 5(T_{\text{on}} + T_{\text{off}})} \tag{10}$$

TABLE I
COMPARISON OF DIFFERENT CONTROL METHODS FOR SWITCHED-CAPACITOR CONVERTER

Description	Open-loop Control	PI Control	VSC method [9]	CVFOCC
Control Type	Linear	Linear	Nonlinear	Nonlinear
Control Method	/	Constant Frequency	Constant Frequency	Variable Frequency
Topology	Simple	Simple	Complex	Simple
Response Time	/	Several switching cycles	Several switching cycles	Immediately
Operation Range	Large	Narrow	Middle	Large
Operation Condition	No limited	Limited	Limited	No Limited
Regulation	Poor	Normal	Good	Good
SC Converters	Low and high power	Low and high power	Low power	Low and high power

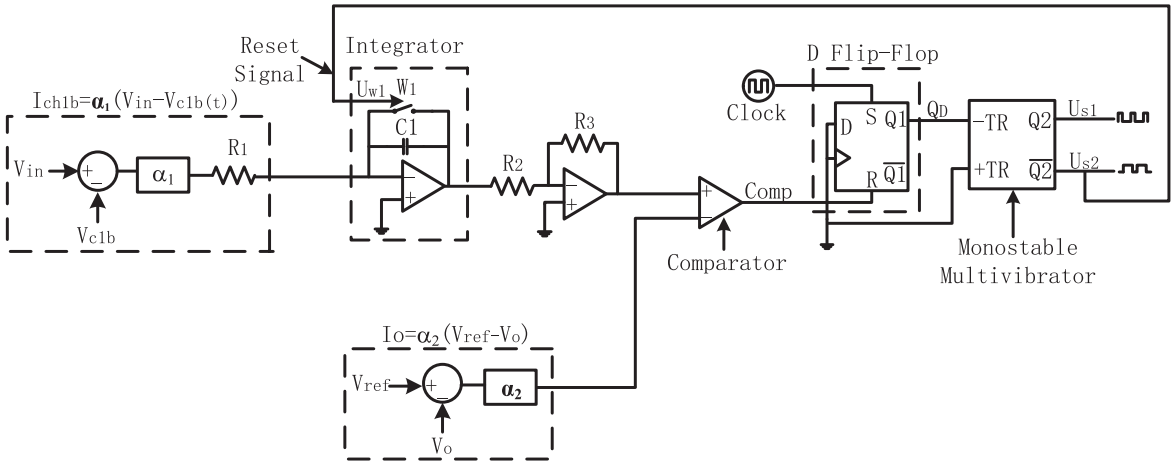

Fig. 4. CVFOCC controller for 3X TBSC converter.

B. Comparison With Other Control Methods

The CVFOCC method is based on the dynamic capacitor ampere-second balance transient calculation modeling method and OCC technique. The dynamical states of a SC converter are instantaneously reflected by the key control equation. Thanks to the resettable integrator and the D flip-flop, which clears the memory states of CVFOCC controller in each switching cycle. Whenever the external disturbance occurs in the input voltage or in the load current, it can be immediately rejected by adjusting the switching frequency during single switching cycle. There is no steady-state error or dynamic error between the average integration value (the charge of flying capacitor) and the negative discharge of flying capacitor. In comparison, the PI control method and the VSC method in [12] used for SC converters adopt the same structure as the conventional PWM voltage-mode controller, but an additional current sensor for construction of control signal and two sets of auxiliary circuits for generation of the ramp signals are used in VSC circuit [12]. The historical states in both control methods need to be considered and compared with the new control signal to adjust the duty cycle to handle external disturbance [38]. As a result, their dynamic response time is longer than the CVFOCC method. The detailed comparison with other control methods is shown in Table I. On the other hand, the proposed control method is a general control method, which is suitable for the low and high-power SC converters.

C. CVFOCC Controller for 3X TBSC Converter

The CVFOCC controller for 3X TBSC converter is shown in Fig. 4 based on (8). It is comprised of a resettable integrator, a comparator, a D flip-flop, a monostable multivibrator, a power source system [including positive dc voltage converter (+5 V) and negative voltage inverter (–5 V)], and some other passive components. The monostable multivibrator acts as the generator of PWM control signals U_{s1} and $U_{s2}(\overline{U_{s1}})$ for switches S_1 and S_2 as shown in Fig. 1. The concept of CVFOCC technique is originated from [27], where four forms of OCC method were proposed. However, the modeling method, implementation circuit, and feedback parameters for 3X TBSC converter are quite different.

As shown in Fig. 4, at the beginning of each switching cycle, the clock signal state sets the D flip-flop high state ($Q1 = 1, \overline{Q1} = 0$). The monostable multivibrator will generate a constant pulse width square signal $U_{s1}(Q2 = U_{s1} = 1, \overline{Q2} = U_{S2} = U_{W1} = 0)$ (constant T_{on} time period) when the falling edge of Q_D signal of D flip-flop arrives. The constant pulse width square signal will turn ON switch S_1 in Fig. 1. While, the control signal U_{W1} will turn OFF the reset switch W_1 of resettable integrator in Fig. 4. The switch S_2 in Fig. 1 will be simultaneously turned OFF by the control signal U_{s2}. The charging current of C_{1b} ($I_{ch1b}(t)$) is integrated by the resettable integrator for constant T_{on} time period. When T_{on} is over, the monostable multivibrator is reset low state ($Q2 = U_{s1} = 0$,

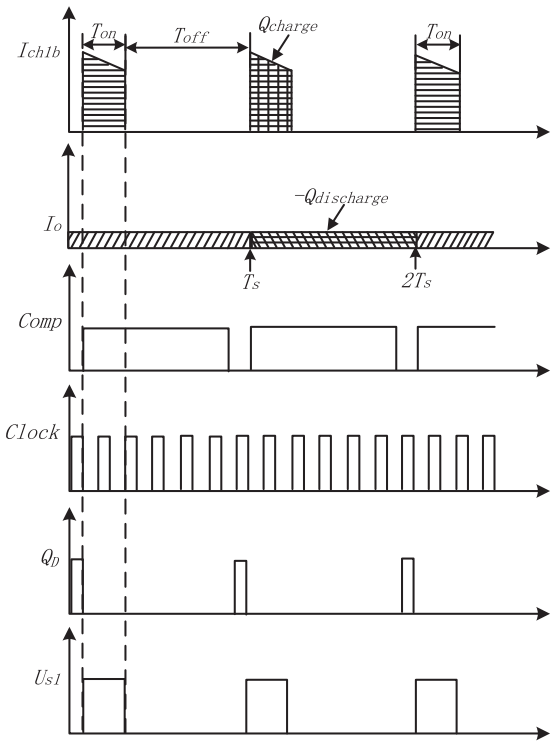

Fig. 5. Operation waveforms of CVFOCC controller.

$\overline{Q2} = U_{S2} = U_{W1} = 1$). At this time point, the reset switch W_1 is turned ON and the resettable integrator in Fig. 4 is reset to zero. The switch S_2 in Fig. 1 will be concurrently turned ON by the control signal U_{s2}. For T_{off} time period, when the negative discharge of $C_{1b}(-Q_{\text{discharge}})$ reaches the charge amount of $C_{1b}(Q_{\text{charge}})$, the comparator in Fig. 4 will change its state from high to low. When the next clock signal arrives, the D flip-flop will be set to high state ($Q1 = 1, \overline{Q1} = 0$) again. When trailing edge of Q_D signal of D flip-flop arrives, the monostable multivibrator will then generate a constant pulse width square signal U_{s1} $(Q2 = U_{s1} = 1, \overline{Q2} = U_{S2} = U_{W1} = 0)$ (constant T_{on} time period) for the new switching cycle. External disturbance can be rejected by adjusting the length of T_{off} time period. The operation waveforms for this configuration can be seen in Fig. 5.

As shown in Fig. 5, when the falling edge of Q_D signal of D flip-flop arrives, a constant pulse width square signal $U_{s1}(U_{s1} = 1, U_{W1} = U_{S2} = 0)$ (constant T_{on} time period) for switch S_1 in Fig. 1 is generated by the monostable mulitivibrator. The charging current of C_{1b} ($I_{\text{ch1}b}(t)$) will be integrated by the resettable integrator for T_{on} time period. At the end of T_{off} time period, when the negative discharge of $C_{1\text{b}}$ $(-Q_{\text{discharge}})$ reaches the charge of $C_{1\text{b}}(Q_{\text{charge}})$ the state of output signal of comparator (Comp) in Fig. 4 changes from high to low. When the next falling edge of Q_D signal of D flip-flop reaches, a new constant pulse width square signal $U_{s1}(U_{s1} = 1, U_{W1} = U_{S2} = 0)$ (constant T_{on} time period) for switch S_1 will be generated by monostable multivibrator. The resettable integrator will be turned on again for the new switching cycle. As a result, the PWM control signal U_{s1} for switch S_1 in Fig. 1 will have constant "on time."

TABLE II
EXPERIMENTAL COMPONENTS PARAMETERS

Component	Type	Value
S_1 (FQA40N25)	N-channel	40 A, 250 V, $R_{DS}(\text{on}) = 70\ \text{m}\Omega$
S_2 (IRFB4332PbF)	N-channel	60 A, 250 V, $R_{DS}(\text{on}) = 29\ \text{m}\Omega$
$D_{1a} \sim D_{2b}$(STTH2002C)	High efficiency ultrafast diode	$I_F = 30$ A,$V_{RRM} = 200$ V $t_{rr} = 22$ nS,$R_d = 10$ m
$C_{1a} \sim C_{2b}$	Film capacitor	450 V,100 100 μF

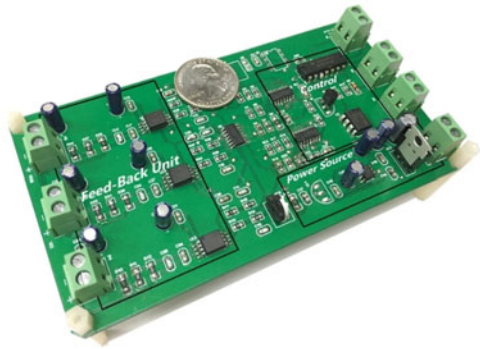

Fig. 6. Annotated photograph of experimental prototype of CVFOCC control board, with an U.S. Quarter added for perspective.

On the other hand, the control PWM signal U_{s2} for switch S_2 in Fig. 1 will have the constant "off time."

The constant "on time" of switch S_1 is determined by the monostable multibrivator. If the "on time" T_{on} of switch S_1 is set less than the time constant τ of charge loop of $C_{1\text{b}}$, the regulation of 3X TBSC converter can be controlled by only adjusting T_{off} time period of switch S_1. As a result, the 3X TBSC converter can work in a wide operation range robustly.

IV. SIMULATION AND EXPERIMENTAL RESULTS

Based on the 3X TBSC converter, the operation performance of CVFOCC method was tested. A 1 KW 3X TBSC converter was designed to operate with the input voltage range 100–120 V. The output voltage is regulated to be 295V and the constant "on time" T_{on} is designed to be 5 μs.The frequency of clock signal for D flip-flop is 100 KHz, and the duty cycle is 0.2. The simulation and experiment parameters of 3X TBSC converter are shown in Table II. An experimental CVFOCC controller prototype was developed as shown in Fig. 6 (based on the controller model in Fig. 4).

A. Comparison With Other Control Methods

Fig. 7 shows the simulation waveforms of output voltage V_o and load current I_o of 3X TBSC converter. Fig. 7(a) and (b) represents the results of proposed CVFOCC method, whereas Fig. 7(c) and (d) shows the PI control method results (bandwidth and switching frequency are 1 KHz and 100 KHz, respectively), and Fig. 7(e) and (f) gives the open-loop control method for side by side comparison. The converter operates at input

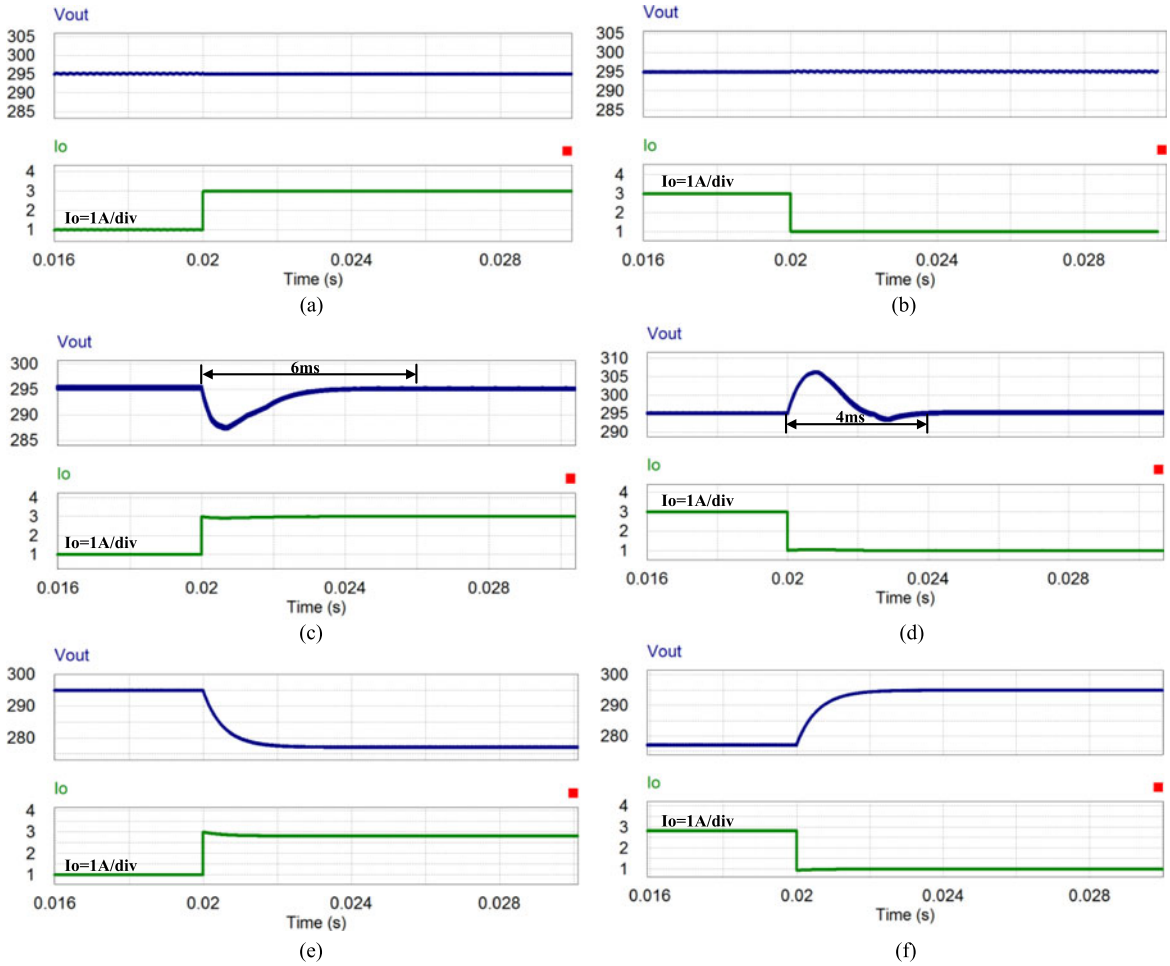

Fig. 7. Comparison of three different control methods with the load resistance of 3X TBSC converter alternating between 295.00 and 98.33 Ω, at input voltage 100 V. (a) Load changes from 295.00 to 98.33 Ω with CVFOCC control method; (b) Load changes from 98.33 to 295.00 Ω with CVFOCC control method; (c) Load changes from 295.00 to 98.33 Ω with PI control method; (d) Load changes from 98.33 to 295.00 Ω with PI control method; (e) Load changes from 295.00 to 98.33 Ω with the open-loop control method; (f) Load changes from 98.33 to 295.00 Ω with the open-loop control method.

voltage of 100 V with load resistance stepping between 295.00 and 98.33 Ω (power level alternates between 295 and 885 W). With the open-loop control method, the output voltage of 3X TBSC converter is not maintained after the transient point. It experiences 16 V voltage drop and 16 V voltage increase as shown in Fig. 7(e) and (f), respectively. By employing PI control method, as shown in Fig. 7(c) and (d), the response time to reject the load current step-up disturbance and load current step-down disturbance are 6.0 and 4.0 ms, respectively. Compared to the aforementioned two control methods, with CVFOCC method, as shown in Fig. 7(a) and (b), the disturbance in load current is immediately rejected with nearly unnoticeable impact at transient time point. Therefore, the advantage of CVFOCC technique for dynamical performance is demonstrated.

B. Dynamic External Disturbance Rejection

The dynamical performance of 3X TBSC in handling load disturbance was—investigated by simulation and experiment by using—the proposed control method and open-loop control method. As shown in Fig. 8(a)–(d), with proposed control method, the load step-up and step-down disturbances (power level alternating between 590 and 885 W) are immediately rejected with small voltage overshoot. Moreover, it can be observed that the experimental results [see Fig. 8(c) and (d)] agree well with the simulated results [see Fig. 8(a) and (b)]. On the other hand, the waveforms of load disturbance rejection for 3X TBSC converter with open-loop control are shown in Fig. 8(e) and (f). As shown in Fig. 8(e), the setting time for 3X TBSC converter to deal with load current step-up disturbance is about 4 ms. For load current step-down disturbance as shown in Fig. 8(f), the setting time is about 6 ms. Note that, the output voltage fluctuation is about 20 V at the transient time point.

The operation waveforms of output voltage (V_o), control signals for switches S_1 and S_2 (U_{s1} and U_{s2}), and input current ($I_{\rm in}$) of 3X TBSC converter are presented in Fig. 9 with CVFOCC method. Two power levels of 3X TBSC converter are, respectively, tested as shown in Fig. 9(a) ($\rm V_{in} = 120$ V, $\rm I_o = 2$ A) and Fig. 9(b) ($\rm V_{in} = 100$ V, $\rm I_o = 3$ A). Note that the switching frequency of Fig. 9(b) is higher than Fig. 9 (a), which is due to higher load and smaller input voltage conditions. It can be seen from Fig. 9, the output voltage can be rigorously maintained with different input voltages and load current by only adjusting the switching frequency.

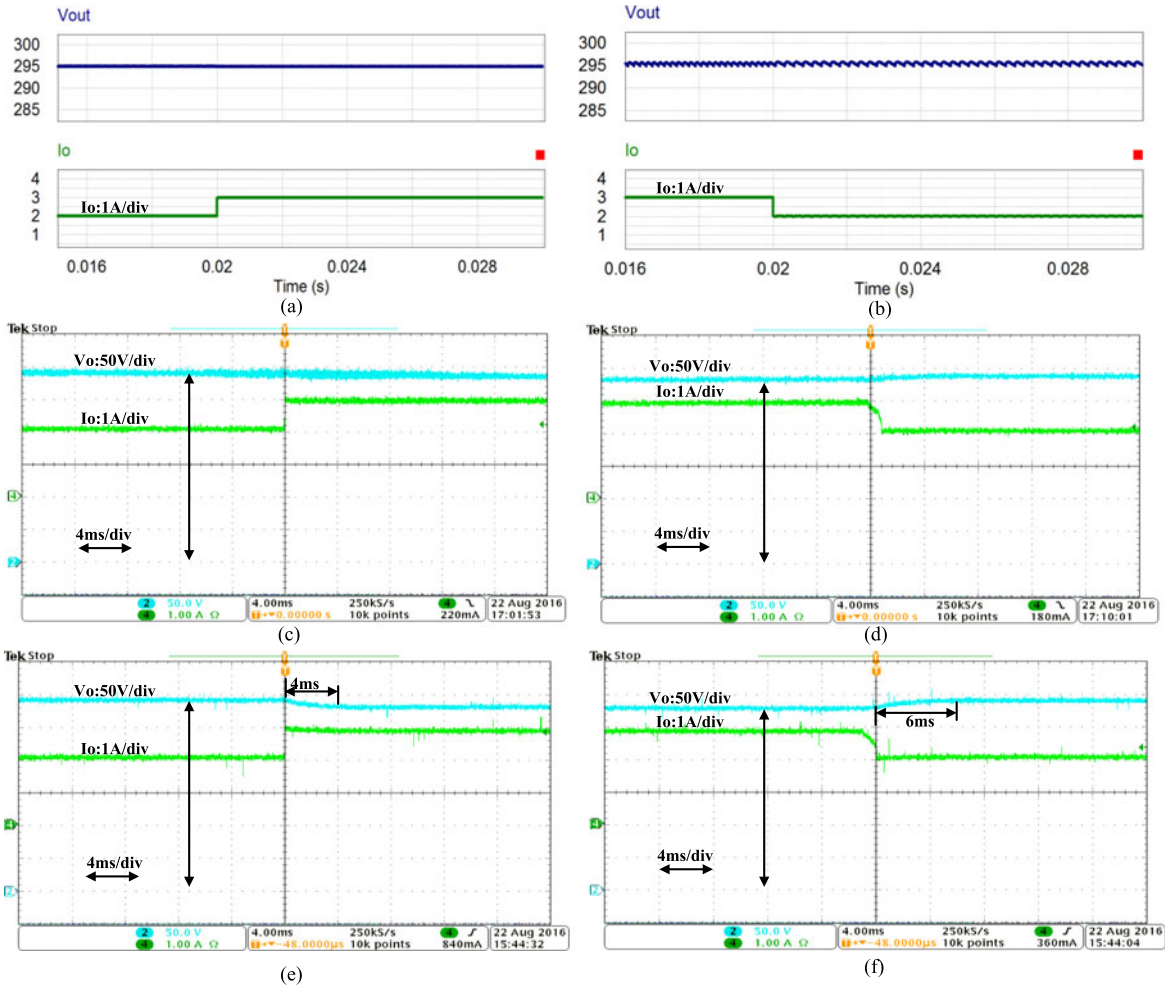

Fig. 8. Operation waveforms of output voltage and load current at input voltage 100 V and 120 V with load resistance alternating between 98.33 Ω and 147.50 Ω, (a) and (c) load current step-up disturbance with proposed control method at input voltage 100 V; (b) and (d) Load current step-down disturbance with the proposed control method at input voltage 120 V; (e) Load step-up disturbance with the open-loop control method at input voltage 100 V; (f) Load step-down disturbance with the open-loop control method at input voltage 120 V.

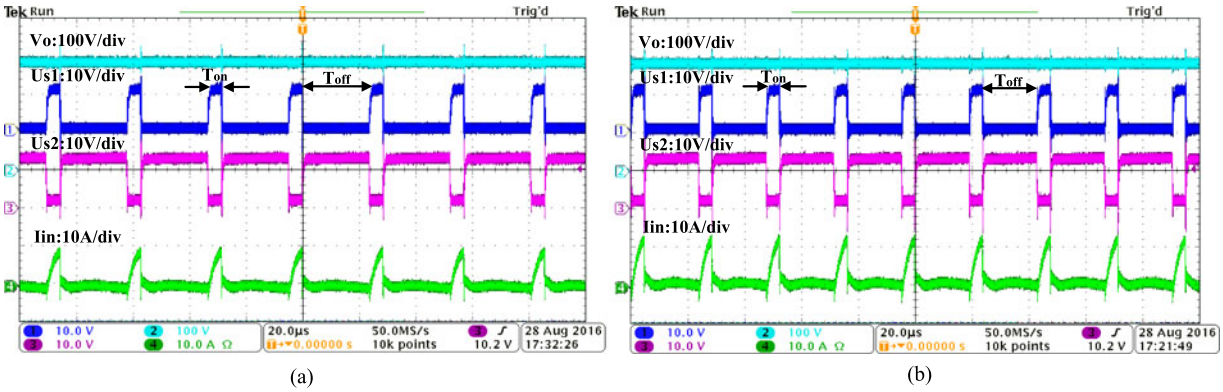

Fig. 9. Operation waveforms of output voltage V_o, control signals U_{s1} and U_{s2} for swiches S_1 and S_2, and input current I_{in} (a) input voltage 120 V and load current 2 A, (b) input voltage 100 V and load current 3 A.

As a result, the fast dynamical response speed of proposed control method to reject external disturbance in power source and load current of high-power 3X TBSC converter is solid verified.

C. Steady-State Performance

To verify the regulation capacity of 3X TBSC converter with the proposed control method, the output voltage, input current versus variable load currents operating at input voltage of 100 V

TABLE III
EXPERIMENTAL AND SIMULATION MEASURED RESULTS

Load (Ω)	Iout(A) (exp)	Iout(A) (sim)	Vin(V)	Iin(A) (exp)	Iin(A) (sim)	Vo(V) (exp)	Error(%) (exp)	Vo(V) (sim)	Error (%) (sim)
640.000	0.460	0.460	100	1.390	1.381	294.50	0.160%	294.260	0.250%
320.000	0.913	0.920	100	2.740	2.764	294.00	0.339%	294.240	0.258%
213.333	1.361	1.379	100	4.050	4.145	292.10	0.644%	294.230	0.339%
164.000	1.790	1.786	100	5.350	5.358	293.7	0.441%	294.20	0.271%
132.000	2.201	2.230	100	6.568	6.695	293.1	0.645%	293.950	0.356%
98.333	2.952	2.984	100	8.951	9.013	292.785	0.751%	293.435	0.531%

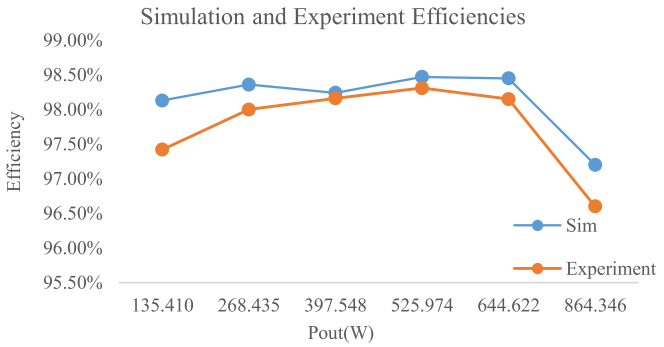

Fig. 10. Plots of efficiency measured by simulation and experiment for CVFOCC controlled 3X TBSC converter.

were measured. Table III shows the data that is obtained from experiment and simulation. As shown in Table III, the largest output voltage errors (compared to the reference voltage 295 V) in experiment and simulation are 0.751% and 0.531%, respectively. Therefore, the good line and load regulation capability of proposed control method is confirmed.

D. Efficiency

The efficiency of 3X TBSC converter under various switching frequency and power levels was also tested at input voltage of 100 V. The input current and load current were measured using the high accuracy Tektronix Current Probe (TCP A300) and Tektronix Oscilloscope (DPO 3014 Digital Phosphor Oscilloscope). On the other hand, input voltage and output voltage were tested by high-accuracy digital multimeter. The measured efficiency curves are shown in Fig. 10. The peak efficiencies in simulation and experiment are 0.9847 and 0.9831, respectively, at load power 525 W.

V. CONCLUSION AND DISCUSSIONS

This paper presents a CVFOCC method for regulation purpose of high-power TBSC converter. It is based on dynamic capacitor ampere-second balance transient calculation modeling method and OCC technique. This control method is robust since the external disturbance can be immediately rejected by adjusting the effective switching frequency while keeping the "on time" constant. Simulation and experimental results show that CVFOCC method has significantly improved the dynamic response speed of high-power SC converter compared to other linear constant frequency control methods. The control loop is straightforward yet provides good line and load regulation. Moreover, the proposed CVFOCC method is a general control method which can be extended for applications of other high-power SC converters.

APPENDIX

In one switching cycle, the maximum and minimum voltages of C_{1a} are given as follows:

$$V_{c1a\max} = V_{\text{in}} - \frac{V_o T_s}{\left(1 - e^{\frac{-T_{\text{off}}}{R_{\text{ch}} C}}\right) R_L C} + \frac{V_o T_s}{R_L C} \tag{11}$$

$$V_{c1a\min} = V_{\text{in}} - \frac{V_o T_s}{\left(1 - e^{\frac{-T_{\text{off}}}{R_{\text{ch}} C}}\right) R_L C}. \tag{12}$$

State 1 in Fig. 2(a) is the only charging period for C_{2a}. In this period, the voltage across C_{2a} rises from minimum value $V_{c2a\min}$ to maximum value $V_{c2a\max}$. Based on KVL, the following equation could be derived as:

$$V_{c2a(t)} - R_{\text{dis}} C \frac{dV_{c1a}(t)}{dt} - V_{c1a}(t) = 0. \tag{13}$$

Considering Kirchhoff's Current Law (KCL) and topology of 3X TBSC converter, the following equation can be derived:

$$C\left(\frac{dV_{c1a}(t)}{dt} + \frac{dV_{c2a}(t)}{dt}\right) = -I_o. \tag{14}$$

Solving (13) and (14) and considering (11) and (12), the maximum and minimum voltages of C_{2a} can be, respectively, written as

$$V_{c2a\max} = V_{\text{in}} - \frac{V_o T_s}{\left(1 - e^{\frac{-T_{\text{off}}}{R_{\text{ch}} C}}\right) R_L C} + \frac{V_o T_s}{R_L C} - \frac{V_o R_{\text{dis}}}{2R_L} \frac{V_o}{R_L C} \left(\frac{(2T_{\text{off}} + T_{\text{on}})}{\left(1 - e^{\frac{-2T_{\text{on}}}{R_{\text{dis}} C}}\right)}\right) + \frac{V_o T_{\text{off}}}{R_L C} \tag{15}$$

$$V_{c2a\min} = V_{\text{in}} - \frac{V_o T_s}{\left(1 - e^{\frac{-T_{\text{off}}}{R_{\text{ch}} C}}\right) R_L C} + \frac{V_o T_s}{R_L C} - \frac{V_o R_{\text{dis}}}{2R_L} \frac{V_o}{R_L C} \left(\frac{(2T_{\text{off}} + T_{\text{on}})}{\left(1 - e^{\frac{-2T_{\text{on}}}{R_{\text{dis}} C}}\right)}\right). \tag{16}$$

Similar to the analysis for C_{2a}, the maximum and minimum voltages of C_{2b} can be derived as

$$V_{c2b\max} = V_{\text{in}} - \frac{V_o T_s}{\left(1 - e^{\frac{-T_{\text{on}}}{R_{\text{ch}}C}}\right) R_L C} + \frac{V_o T_s}{R_L C} - \frac{V_o R_{\text{dis}}}{2R_L}\frac{V_o}{R_L C}\left(\frac{(2T_{\text{on}} + T_{\text{off}})}{\left(1 - e^{\frac{-2T_{\text{off}}}{R_{\text{dis}}C}}\right)}\right) + \frac{V_o T_{\text{on}}}{R_L C} \quad (17)$$

$$V_{c2b\min} = V_{\text{in}} - \frac{V_o T_s}{\left(1 - e^{\frac{-T_{\text{on}}}{R_{\text{ch}}C}}\right) R_L C} + \frac{V_o T_s}{R_L C} - \frac{V_o R_{\text{dis}}}{2R_L}\frac{V_o}{R_L C}\left(\frac{(2T_{\text{on}} + T_{\text{off}})}{\left(1 - e^{\frac{-2T_{\text{off}}}{R_{\text{dis}}C}}\right)}\right). \quad (18)$$

Due to the symmetrical configuration of 3X TBSC converter, the output voltage can be approximately derived as following equation:

$$V_o = \frac{(V_{c2a\max} + V_{c2a\min} + V_{c2b\max} + V_{c2b\min})}{2} + V_{\text{in}}. \quad (19)$$

Substituting (15), (16), (17), and (18) into (19), the voltage gain could be derived as (10).

The similar detailed derivation process for 3X TBSC converter could be found in [24] and [26].

REFERENCES

[1] Y. Lei and R. C. N. Pilawa-Podgurski, "A general method for analyzing resonant and soft-charging operation of switched-capacitor converters," *IEEE Trans. Power Electron.*, vol. 30, no. 10, pp. 5650–5664, May 2015.

[2] S. Xiong, S. C. Wong, S. C. Tan, and C. K. Tse, "A family of exponential step-down switched-capacitor converters and their applications in two-stage converters," *IEEE Trans. Power Electron.*, vol. 29, no. 4, pp. 1870–1880, Oct. 2014.

[3] J. C. Mayo-Maldonado, J. C. Rosas-Caro, and P. Rapisarda, "Modeling approaches for DC–DC converters with switched capacitors," *IEEE Trans. Ind. Electron.*, vol. 62, no. 2, pp. 953–959, Jan. 2015.

[4] S. V. Cheong, H. Chung, and A. Ioinovici, "Duty-cycle control boosts DC-DC converters," *IEEE Circuits Devices Mag.*, vol. 9, no. 2, pp. 36–37, Mar. 1993.

[5] S. V. Cheong, H. S. H. Chung, and A. Ioinovici, "Inductorless DC-DC converter with high power density," *IEEE Trans. Ind. Electron.*, vol. 41, no. 2, pp. 208–215, Apr. 1994.

[6] L. Fu, X. Zhang, F. Guo, and J. Wang, "A phase shift controlled current-fed quasi-switched-capacitor isolated dc/dc converter with GaN HEMTs for photovoltaic applications," in *Proc. IEEE Appl. Power Electron. Conf. Expo.*, Mar. 2015, pp. 191–198.

[7] H. Chung and Y. K. Mok, "Development of a switched-capacitor DC/DC boost converter with continuous input current waveform," *IEEE Trans. Circuits Syst. I Fundam. Theory Appl.*, vol. 46, no. 6, pp. 756–759, Jun. 1999.

[8] H. Chung, S. Y. R. Hui, S. C. Tang, and A. Wu, "On the use of current control scheme for switched-capacitor DC/DC converters," *IEEE Trans. Ind. Electron.*, vol. 47, no. 2, pp. 238–244, Apr. 2000.

[9] H.-K. Kwan, D. C. W. Ng, and V. W. K. So, "Design and analysis of dual-mode digital-control step-up switched-capacitor power converter with pulse-skipping and numerically controlled oscillator-based frequency modulation," *IEEE Trans. Very Large Scale Integr. Syst.*, vol. 21, no. 11, pp. 2132–2140, Nov. 2013.

[10] T. Souvignet, B. Allard, and S. Trochut, "A fully integrated switched-capacitor regulator with frequency modulation control in 28-nm FD-SOI," *IEEE Trans. Power Electron.*, vol. 31, no. 7, pp. 4984–4994, Jul. 2016.

[11] W. C. Chen, D. L. Ming, Y. P. Su, Y. H. Lee, and K. H. Chen, "A wide load range and high efficiency switched-capacitor DC-DC converter with pseudo-clock controlled load-dependent frequency," *IEEE Trans. Circuits Syst. I, Reg. Papers*, vol. 61, no. 3, pp. 911–921, Mar. 2014.

[12] S. C. Tan, S. Bronstein, M. Nur, Y. M. Lai, A. Ioinovici, and C. K. Tse, "Variable structure modeling and design of switched-capacitor converters," *IEEE Trans. Circuits Syst. I, Reg. Papers*, vol. 56, no. 9, pp. 2132–2142, Sep. 2009.

[13] S. C. Tan, S. Bronstein, M. Nur, Y. M. Lai, A. Ioinovici, and C. K. Tse, "Nonlinear control of switched-capacitor converter using sliding mode control approach," in *Proc. 2008 IEEE Power Electron. Spec. Conf.*, Rhodes, IA, USA, Jun. 2008, pp. 372–377.

[14] M. S. Makowski and D. Maksimovic, "Performance limits of switched-capacitor DC-DC converters," in *Proc. IEEE Power Electron. Spec. Conf.*, Atlanta, GA, USA, Jun. 1995, vol. 2, pp. 1215–1221.

[15] S. C. Tan, S. Kiratipongvoot, S. Bronstein, A. Ioinovich, Y. M. Lai, and C. K. Tse, "Adaptive mixed on-time and switching frequency control of a system of interleaved switched-capacitor converters," *IEEE Trans. Power Electron.*, vol. 26, no. 2, pp. 364–380, Feb. 2011.

[16] F. Zhang, L. Du, F. Z. Peng, and Z. Qian, "A new design method for high power high-efficiency switched-capacitor DC–DC converters," *IEEE Trans. Power Electron.*, vol. 23, no. 2, pp. 832–840, Mar. 2008.

[17] D. Flores Cortez, G. Waltrich, J. Fraigneaud, H. Miranda, and I. Barbi, "DC–DC converter for dual-voltage automotive systems based on bidirectional hybrid switched-capacitor architectures," *IEEE Trans. Ind. Electron.*, vol. 62, no. 5, pp. 3296–3304, May 2015.

[18] W. Qian, H. Cha, F. Z. Peng, and L. M. Tolbert, "55-kW variable 3X DC–DC converter for plug-in hybrid electric vehicles," *IEEE Trans. Power Electron.*, vol. 27, no. 4, pp. 1668–1678, Apr. 2012.

[19] L. A. Romero, T. B. Lazzarin, and I. Barbi, "A 1 kW step-Up/step-down switched-capacitor AC–AC converter," *IEEE Trans. Power Electron.*, vol. 28, no. 7, pp. 3329–3340, Jul. 2013.

[20] M. D. Vecchia, T. B. Lazzarin, and I. Barbi, "A three-phase AC–AC converter in open-delta connection based on switched-capacitor principle," *IEEE Trans. Ind. Electron.*, vol. 62, no. 10, pp. 6035–6041, Oct. 2015.

[21] F. Z. Peng, F. Zhang, and Z. Qian, "A magnetic-less DC–DC converter for dual-voltage automotive systems," *IEEE Trans. Ind. Appl.*, vol. 39, no. 2, pp. 511–518, Mar./Apr. 2003.

[22] K. Zou, M. J. Scott, and J. Wang, "A switched-capacitor voltage tripler with automatic interleaving capability," *IEEE Trans. Power Electron.*, vol. 27, no. 6, pp. 2857–2868, Jun. 2012.

[23] W. Qian, D. Cao, J. G. C. Rivera, M. Gebben, D. Wey, and F. Z. Peng, "A switched-capacitor DC–DC converter with high voltage gain and reduced component rating and count," *IEEE Trans. Ind. Electron.*, vol. 48, no. 4, pp. 1397–1406, Jul. 2012.

[24] B. Wu, S. xiang Li, K. M. Smedley, and S. Singer, "Analysis of high power switched capacitor converter regulation based on charge-balance transient-calculation method," *IEEE Trans. Power Electron.*, vol. 31, no. 5, pp. 3482–3494, Dec. 2015.

[25] B. Wu, S. Keyue, and S. Sigmond, "A new 3X interleaved bidirectional switched capacitor converter," in *Proc. IEEE Appl. Power Electron. Conf. Expo.*, 2014, pp. 1433–1439.

[26] B. Wu, S. Li, K. Smedley, and S. Singer, "A family of two-switch boosting switched-capacitor converters," *IEEE Trans. Power Electron.*, vol. 30, no. 10, pp. 5413–5424, Oct. 2015.

[27] K. M. Smedley and S. Cuk, "One-cycle control of switching converters," *IEEE Trans. Power Electron.*, vol. 10, no. 6, pp. 625–633, Nov.1995.

[28] N. Vamanan and V. John, "Dual comparison one cycle control for single phase AC to DC converters," *IEEE Trans. Ind. Appl.*, vol. 52, no. 4, pp. 3267–3278, Jul./Aug. 2016.

[29] E. S. Sreeraj, E. K. Prejith, K. Chatterjee, and S. Bandyopadhyay, "An active harmonic filter based on one-cycle control," *IEEE Trans. Ind. Electron.*, vol. 61, no. 8, pp. 3799–3809, Aug. 2014.

[30] M. Tedde and K. Smedley, "Anti-islanding for three-phase one-cycle control grid tied inverter," *IEEE Trans. Power Electron.*, vol. 29, no. 7, pp. 3330–3345, Jul. 2014.

[31] A. A. de Melo Bento, P. K. P. Vieira, and E. R. C. da Silva, "Application of the one-cycle control technique to a three-phase three-level NPC rectifier," *IEEE Trans. Ind. Appl.*, vol. 50, no. 2, pp. 1177–1184, Mar. 2014.

[32] J. M. Henry and J. W. Kimball, "Practical performance analysis of complex switched-capacitor converters," *IEEE Trans. Power Electron.*, vol. 26, no. 1, pp. 127–136, Jan. 2011.

[33] J. M. Henry and J. W. Kimball, "Switched-capacitor converter state model generator," *IEEE Trans. Power Electron.*, vol. 27, no. 5, pp. 2415–2425, May 2012.

[34] M. Evzelman and S. Ben-Yaakov, "Average-current-based conduction losses model of switched capacitor converters," *IEEE Trans. Power Electron.*, vol. 28, no. 7, pp. 3341–3352, Jul. 2013.
[35] S. Ben-Yaakov, "Behavioral average modeling and equivalent circuit simulation of switched capacitors converters," *IEEE Trans. Power Electron.*, vol. 27, no. 2, pp. 632–636, Feb. 2012.
[36] M. D. Seeman and S. R. Sanders, "Analysis and optimization of switched-capacitor dc–dc converters," *IEEE Trans. Power Electron.*, vol. 23, no. 2, pp. 841–851, Mar. 2008.
[37] L. Muller and J. Kimball, "A dynamic model of switched-capacitor power converters," *IEEE Trans. Power Electron.*, vol. 29, no. 4, pp. 1862–11869, Apr. 2014.
[38] W. Li, L. Liang, W. Liu, and X. Wu, "State of charge estimation of lithium-ion batteries using a discrete-time nonlinear observer," *IEEE Trans. Power Electron.*, vol. PP, no. 99, pp. 1–1.

Bin Wu (S'14) was born in Zhejiang, China, 1985. He received the B.S degree in electrical engineering from Zhejiang University, Hangzhou, China, in 2008, the M.S. degree in power electronics from Xi'an Jiao tong University, Xi'an, China, in 2011, and the Ph.D. degree in electrical engineering from the University of California, Irvine, CA, USA, in 2016.

From 2016 to 2017, he works as a Postdoctoral Research Associate at the University of Maryland, College Park, MD, USA. He is currently with Battery Management Division in Maxim Integrated, San Jose, CA, USA. His interests include switched capacitor converter, modeling, high gain dc–dc converter, electrical vehicle, and renewable energy integration.

Lei Yang (S'15) was born in Henan, China, in 1986. He received the B.S degree in electric and information engineering from the Information Engineering University, Zhengzhou, China, in 2011, the M.S. degree in signal and information processing and the Ph.D. degree in electrical engineering in April 2014 and in June 2017,respectively, both from Northwestern Polytechnical University, Xi'an, China.

He is currently working as an Assistant Professor at Xi'an University of Technology, Xi'an, China. From September 2014 to September 2016, he had been studied as a Visiting Student at the University of California, Irvine, CA, USA. His research interests include nonlinear control, switched–capacitor converter, dc–dc converter, power source of electrical vehicle, and renewable energy integration.

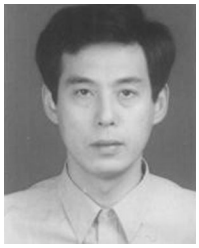

Xiaobin Zhang received the B.S. and M.S degrees in electrical engineering from the School of Automation, Northwestern Polytechnical University, Xi'an, China, in 1983 and 1986, respectively.

Since 1986, he has been with the School of Automation, Northwestern Polytechnical University, Xi'an, China, where he is currently a Professor. His research interests include power electronic control, aircraft power system, multipulse converter, and power decoupling

Keyue Ma Smedley (S'87–M'90–SM'97–F'08) received the B.S. and M.S. degrees in electrical engineering from Zhejiang University, Hangzhou, China, in 1982 and 1985, respectively, and the M.S. and Ph.D. degrees in electrical engineering from California Institute of Technology, Pasadena, CA, USA, in 1987 and 1991, respectively.

She is currently a Professor in the Department of Electrical Engineering and Computer Science, University of California, Irvine (UCI), Irvine, CA, USA, the Director of the UCI Power Electronics Laboratory, and a Cofounder of One-Cycle Control, Inc. She is an Inventor of One-Cycle Control and the Hexagram power converter. She work has resulted in more than 160 technical publications, more than 10 U.S./international patents, two startup companies, and numerous commercial applications. Her research interests include high-efficiency dc–dc converters, high-fidelity class-D power amplifiers, single-phase and three-phase PFC rectifiers, active power filters, inverters, V/VAR control, energy storage system, and utility-scale fault current limiters.

Dr. Smedley received the UCI Innovation Award 2005. Her work with One-Cycle Control, Inc., has won Department of the Army Achievement Award in the Pentagon in 2010.

Guann-Pyng Li (M'83) received the B.S. degree in electrical engineering from the National Cheng Kung University (NCKU), Tainan, Taiwan, in 1978 and the M.S. and Ph.D. degrees in electrical engineering from the University of California, Los Angeles (UCLA), Los Angeles, CA, USA, in 1982 and 1983 respectively.

He is currently a Professor at the University of California, Irvine, CA, USA, with appointments in three departments: Electrical Engineering and Computer Science, Chemical Engineering and Materials Science, and Biomedical Engineering. At University of California, Irvine, he also serves as the Division Director of the California Institute for Telecommunications and Information Technology (Calit2) and the Director of the Integrated Nano systems Research Facility in Henry Samueli School of Engineering. He currently holds 25 U.S. patents and has 15 patents pending. He has published more than 320 research papers involving microelectronic technologies, microwave circuit design, microelectromechanical systems for communication and biomedical instrumentation applications, and bionano-IT technology.